J Nanopart Res (2017) 19: 54
DOI 10.1007/s11051-017-3766-1

RESEARCH PAPER

A comparative study of alumina-supported Ni catalysts prepared by photodeposition and impregnation methods on the catalytic ozonation of 2,4-dichlorophenoxyacetic acid

Julia L. Rodríguez · Miguel A. Valenzuela · Hugo Tiznado · Tatiana Poznyak · Isaac Chairez · Diana Magallanes

Received: 14 October 2016 / Accepted: 24 January 2017 / Published online: 6 February 2017

Abstract The heterogeneous catalytic ozonation on unsupported and supported oxides has been successfully tested for the removal of several refractory compounds in aqueous solution. In this work, alumina-supported nickel catalysts prepared by photodeposition and impregnation methods were compared in the catalytic ozonation of 2,4-dichlorophenoxyacetic acid (2,4-D). The catalysts were characterized by high-resolution electron microscopy and X-ray photoelectron spectroscopy. The photochemical decomposition of Ni acetylacetonate to produce $Ni(OH)_2$, NiO, and traces of Ni° deposited on alumina was achieved in the presence of benzophenone as a sensitizer. A similar surface composition was found with the impregnated catalyst after its reduction with hydrogen at 500 °C and exposed to ambient air. Results indicated a higher initial activity and maleic acid (byproduct) concentration with the photodeposited catalyst (1 wt% Ni) compared to the impregnated catalyst (3 wt% Ni). These findings suggest the use of the photodeposition method as a simple and reliable procedure for the preparation of supported metal oxide/metal catalysts under mild operating conditions.

Keywords Catalytic ozonation · 2,4-D · Nickel nanoparticles · Alumina · Photodeposition · Impregnation

J. L. Rodríguez · T. Poznyak · D. Magallanes
Lab. Ing. Química Ambiental. ESIQIE–Instituto Politécnico Nacional, Zacatenco, 07738, México, D.F, Mexico

J. L. Rodríguez (✉) · M. A. Valenzuela
Lab.Catálisis y Materiales. ESIQIE–Instituto Politécnico Nacional. Zacatenco, 07738, México, D.F, Mexico
e-mail: ozliliana@yahoo.com.mx

H. Tiznado
Centro de Nanociencias y Nanotecnología. CNyN Universidad Nacional Autónoma de México, Km. 107 Carretera Tijuana a Ensenada, 22860 Ensenada, Baja California, Mexico

I. Chairez
Departamento de Bioprocesos, UPIBI- Instituto Politécnico Nacional, Ticoman, 07340, México, D.F, Mexico

Introduction

The advanced oxidation processes (AOPs) have been extensively studied in the last two decades, to be included in modern industrial wastewater treatment schemes for improving water biodegradation and its final quality (Qi et al. 2008; Pocostales et al. 2011; Yang et al. 2009). Generally, AOPs generate hydroxyl radicals in adequate amount to degrade the contaminants (Gautam and Chattopadhyaya 2016). The catalytic ozonation belongs to the group of AOP used in the degradation of toxic organic compounds, and its main characteristic is the high efficiency achieved in the degradation and mineralization of a variety of refractory organic pollutants in water (Nie et al. 2013; Ernst et al. 2004; Ikhlaq et al. 2012; Qi et al. 2013). It was conceived to overcome the drawbacks of conventional ozonation, such as accumulation of intermediates, selective ozone reactions, and high ozone consumption (Nawrocki 2013).

The catalytic ozonation with metal oxides has shown to enhance the degradation of recalcitrant compounds in water (Avramescu et al. 2008; Zhang et al. 2012). Generally, two mechanisms are proposed during catalytic ozonation: (i) ozone decomposition on the catalyst surface improving the hydroxyl radical (·OH) generation, where the hydroxyl groups are the active sites and (ii) the generation of metal-organic compound complexes on the catalyst surface, which are easily eliminated with ozone (Zhang et al. 2012; Nawrocki and Kasprizk-Hordern 2010). Various studies have focused on the use of supported metal/metal oxide or unsupported alumina in water treatment by catalytic ozonation (Pocostales et al. 2011; Ernst et al. 2004; Rosal et al. 2010; Yang et al. 2010). These works have shown that the chemical and structural modification of alumina and composites have a positive effect in the degradation and mineralization of organic pollutants. For instance, Qi et al. 2008 demonstrated that the highest activity of alumina takes place at a similar pH to reach its point of zero charge (pH_{pzc}), which indicates that ozone decomposition occurs on non-charged surface hydroxyl groups. Furthermore, a clear correlation between the density of surface hydroxyl groups and the concentration of hydroxyl radicals (·OH), transformed from ozone, was also revealed (Qi et al. 2008).

Recent research has shown that alumina is a successful material in the catalytic ozonation of pharmaceuticals (Pocostales et al. 2011; Yang et al. 2009; Yang et al. 2010), pesticide (Nie et al. 2013; Guzman-Perez et al. 2012), and refractory organic acids (Ernst et al. 2004). Several reaction mechanisms explaining the role of alumina in the degradation of organic compounds have been proposed by diverse research groups. According to the reports, it seems that the organic pollutant degradation in the presence of alumina can be due to (i) generation of reactive oxygen radicals including hydroxyl radical (·OH) (Qi et al. 2008; Ikhlaq et al. 2012; Qi et al. 2013), (ii) formation of superoxide ion radical/hydrogen peroxide (Ikhlaq et al. 2013), and (iii) adsorption or chelating reaction on the Al oxide surface (Ernst et al. 2004).

Particularly, NiO/Al_2O_3 catalysts have been tested in the degradation of oxalic acid showing an improved removal rate in comparison with the non-catalytic process (Avramescu et al. 2008). In another work, the catalytic ozonation of ammonium ion in water was studied with several metal oxides and it was found the highest oxidative degradation with MgO and NiO, but with a low selectivity (Ichikawa et al. 2014). Recently, we have evidenced that NiO reacts with the toxic pollutant (2,4-D) forming a complex hybrid, which gave rise to a significant mineralization of 2,4-D (Rodríguez et al. 2013).

The development of supported metal nanoparticles has been intensively studied for applications in several fields. In catalysis is of great importance to control the size and shape of the nanoparticles. Lately, we have reported the preparation of nickel oxide supported on SiO_2 with a narrow particle size distribution through a photochemical approach, namely liquid phase photodeposition (LPPD) technique in the presence of a sensitizer (Rodríguez et al. 2014). This method allows the direct deposition of active metallic species on the support from liquid phase at ambient conditions (Scirè et al. 2012; Scirè et al. 2011; Crisafulli et al. 2006). The sensitized photodeposition method implies the addition of a highly active compound in the photochemical processes for the reduction of the metal source. The process is initiated by the sensitizer light absorption that generates a photoexcited state, giving rise to several types of radicals which reduce the metal ions producing metallic nanoparticle cluster able to spread over the support surface (Crisafulli et al. 2006; Scirè et al. 2011). One typical combination in photochemical systems is the ketone derivatives/α-alcohol, where the former is the radical precursor while the α-alcohol works simultaneously as the solvent as hydrogen donor during UV-light irradiation (Sakamoto et al. 2009). Acetone, acetophenone, and benzophenone can generate ketyl radicals, for this reason is widely used as sensitizers (Krylova et al. 2005; Kometani et al. 2002).

Recently, some research groups have synthetized catalysts using alumina as a support by LPPD. Generally, the precursors were metallic β-diketonates complex which were subjected to irradiation in presence of alumina (Crisafulli et al. 2006; Scirè et al. 2011). Crisafulli et al. 2006 prepared Pt catalysts supported on alumina finding a narrow particle size distribution centered around 1.6 nm by LPPD in comparison with a bimodal distribution of 2.8 and 4 nm by using an impregnation method. Similar results were obtained by Scirè et al. 2011 during the preparation of Pd/Al_2O_3 catalyst. However, in this case, the presence of acetone was necessary as sensitizer. With the aim to protect the active phase to oxidation, the presence of unmodified β-cyclodextrin was used as shielding agent for applications in VOC combustion (Scirè et al. 2012).

Taking into account our previous studies in the catalytic ozonation of 2,4-D on unsupported NiO and NiO

supported on SiO_2 or TiO_2 (Rodríguez et al. 2014; Rodríguez et al. 2012), the goal of this research was to compare the role of the preparation method (photodeposition vs impregnation) of NiO nanoparticles supported on Al_2O_3, with respect to their surface and catalytic properties in the degradation of 2,4-D in aqueous solution.

Experimental methods

Materials and reagents

All chemicals were analytical grade and used as received without any further purification: bis(2,4-pentandionato) Ni(II) ($Ni(acac)_2$), benzophenone, oxalic acid obtained from Aldrich, 2,4-dichlorophenoxyacetic acid (Alfa Aesar, 98%), and 2,4-dichlorophenol (Sigma Aldrich, 99%). Anhydrous ethanol (J.T. Baker) was spectrophotometric grade. Al_2O_3-γ nanopowder with particle size <50 nm and surface area >40 m^2/g (Sigma Aldrich) was used as a support.

Catalyst preparation

Liquid phase photodeposition method

A solution of $Ni(acac)_2$ (8×10^{-4} M, 1 wt%) in alcoholic medium with acetone or benzophenone (10^{-3} M), as sensitizers, was used in all the experiments. In the glass reactor, it was also added a dose of Al_2O_3 (0.1 g L^{-1}) at 25 °C and the suspension was purged with nitrogen. During the photoreaction, the suspension was subjected to a vigorous and continuous stirring with the aim to avoid the sedimentation of alumina. The mixture was irradiated with 14 black light UVA lamps (8 W) which have a maximum emission at about 365 nm. After irradiation, the sample was dried at 120 °C to evaporate the solvent. The kinetics of the $Ni(acac)_2$ photodecomposition was performed by using a Lambda UV-Vis spectrophotometer (Perkin Elmer) at a wavelength of 310 nm.

Impregnation method

Ni/Al_2O_3 (I) catalyst was synthetized by the wetness impregnation method mixing Al_2O_3 nanopowder with $Ni(acac)_2$ in ethanol solution (3 wt% nominal). The $Ni(acac)_2$ solution was prepared in a similar way than that used in the photodeposition method ("Liquid phase photodeposition method" section) and it was adsorbed on Al_2O_3 during 24 h. After impregnation, the sample was dried 12 h at 110 °C, calcined during 2 h at 500 °C, and finally reduced 1 h at 500 °C.

Characterization techniques

TEM images were obtained using a JEOL-JEM-2200 field emission operated at 200 kV. The samples were prepared with the catalyst (<1 mg) in methanol and dispersed by ultrasound for 5 min. Thereafter, a drop of the solution was placed over a carbon coated Cu grid (300 mesh) and dried at room temperature.

Photoelectron core-level spectra of the as-prepared samples were obtained with an X-ray photoelectron spectroscopy (XPS) system (ThermoFisher Scientific K-Alpha), with a monochromatized AlKα X-ray source (1487 eV). The base pressure of the system was 10^{-9} mbar. Prior to XPS analysis, all samples were dried at 100 °C for 24 h. Subsequently, they were dispersed and embedded in a 5 × 5-mm indium foil and fixed with Cu double side tape to the sample holder. Narrow scans were collected at 60 eV analyzer pass energy and a 400-μm spot size. The position of the C1s peak at 284.6 eV was monitored on each sample to ensure that no binding energy shift due to charging had occurred. The spectra were decomposed into their components with mixed Gaussian–Lorentzian lines by a non-linear least squares curve-fitting procedure, using the public software package XPSPEAK 4.1. The binding energies and FWHM of the peaks were determined from the fitting results after subtraction of the Shirley-type background. Deconvoluted peak areas and standard sensitivity factors were used to evaluate the surface composition of the samples. The zeta potential of catalysts was determined by Malvern Zeta-Sizer at 25 °C using the titration method with NaOH (0.01 N).

Ozonation procedure

Ozone was generated from dry oxygen by the ozone generator (corona discharge type) HTU500G (AZCO Industries Limited–Canada). The Ozone Analyzer BMT 964 BT (BMT Messtechnik, Berlin) provides on-line ozone monitoring in the gaseous phase at the reactor outlet for the control of the ozonation degree, the ozone consumption, and the ozone decomposition as well. All experiments with ozone were carried out in a

semi-batch type reactor (0.5 L) at 21 °C. The agitation was provided by means of an ozone–oxygen mixture bubbling through a ceramic porous filter, which is placed at the bottom of the reactor. The initial ozone concentration was 25 mg L^{-1}. The ozone–oxygen mixture flow was 0.5 L min^{-1}. The flow diagram of the ozonation procedure is described in our previous publication (Rodríguez et al. 2012).

Analytical methods

The model solution of 2,4-D herbicide was prepared with a concentration of 80 mg L^{-1} at 3.1 initial pH. The catalyst concentration was constant at 0.1 g L^{-1}. Aliquot of 3 mL ozonation reaction solution was withdrawn at time intervals from the reactor for sequent analysis. UV-Vis absorption spectrums of 2,4-D were measured with Lambda UV-Vis spectrophotometer (Perkin Elmer). A HPLC apparatus (Perkin Elmer series 200, UV/Vis detector) was used to record the change of concentration of 2,4-D, under the following operation conditions: Prevail Organic Acid (Grace) with mobile phase of KH_2PO_4 (25 Mm) at pH 2.6 adjusted with phosphoric acid: acetonitrile (60:40) with a flow of 1 mL min^{-1} at wavelength of 225 nm.

Results and discussion

Photochemical deposition of Ni onto Al_2O_3

Diverse researchers have widely used β-metal diketonate complexes as precursors in alcoholic medium by LPPD technique (Scirè et al. 2012; Scirè et al. 2011; Crisafulli et al. 2006). For instance, the generation of metallic copper, nickel, palladium, or platinum was formed by photochemical reaction in solution upon LMCT (ligand to metal charge transfer) excitation or sensitization with triplet, aromatic ketones (Scirè et al. 2012; Scirè et al. 2011; Rodríguez et al. 2012; Scirè et al. 2009; Crisafulli et al. 2006).

Previously, we have reported that the rate constant in the photochemical decomposition of $Ni(acac)_2$ by using benzophenone as sensitizer is one magnitude order higher compared to that of acetone (Rodríguez et al. 2013). The evolution of the $Ni(acac)_2$ normalized concentrations as a function of irradiation time for the photochemical, photosensitized, and photodeposition reaction in the presence of alumina is shown in Fig. 1. As can be seen, the photochemical conversion of the Ni precursor (i.e., only in ethanol solution) was negligible, while its photosensitized conversion with benzophenone addition or benzophenone plus alumina caused a significant decrease of its initial concentration. It is worth noting the increased conversion of the Ni precursor in the presence of alumina, which can be related to the deposition of nickel nanoparticles in the alumina pores avoiding light scattering. On the other hand, the adsorption in the liquid phase of the $Ni(acac)_2$ on alumina generates several metal–alumina interactions, which favors the decomposition of the Ni precursor (Molina and Poncelet 1999).

Note that either with the use of a photosensitizer or low concentration of Ni precursor (8×10^{-4} M), no complete conversion was observed thereof, which means that the formation of intermediates can inhibit the main reaction, as reported by Giuffrida et al. 2007.

$$Ni(acac)_2 \rightarrow^{hv} \overset{\circ}{Ni} + 2Hacac + \text{decomposition products of the solvent}$$

From these results, we conclude that the Ni species coming from the photoreduction of $Ni(acac)_2$ are occluded in the alumina pores and the increasing amount of the reaction byproducts prevent the continuous reduction process. Theoretically, for both, preparation methods should have been obtained Ni° nanoparticles; however, at being in contact with ambient air, they are highly unstable and are transformed into oxides, hydroxides, among others Ni species, which will be analyzed in more detail below with our XPS study.

Catalyst characterization

In order to characterize nickel nanoparticles, transmission electron microscopy was carried out with both, the catalyst synthetized by photodeposition and impregnation methods. Figure 2 reports TEM micrographs and size distribution histograms of alumina-supported nickel nanoparticles.

The bigger spherical particles correspond to alumina, while the smaller particles of geometry almost spherical correspond to nickel species (Ni, NiO, $Ni(OH)_2$), Fig. 2a. These Ni species were not well homogeneously spread over the support surface with an evident formation of embedded aggregates. Regarding the histogram of the size distribution reported in Fig. 2b, it was found

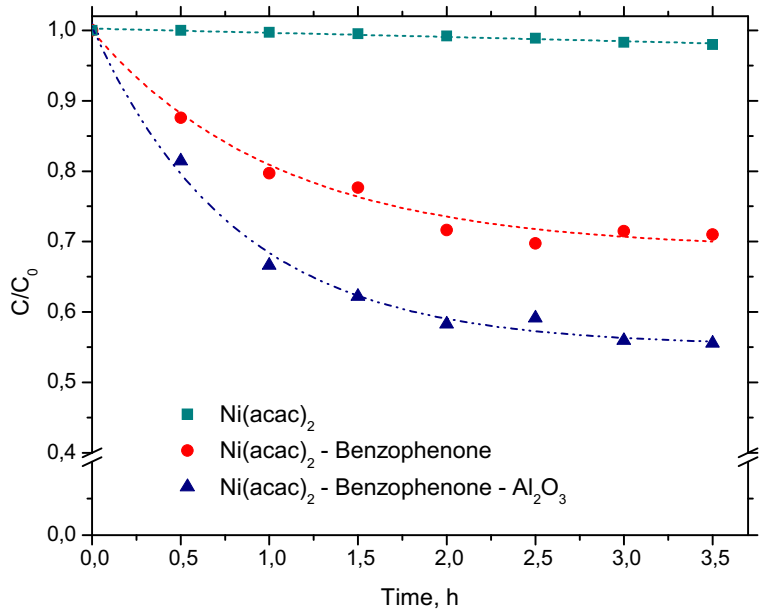

Fig. 1 Dimensionless concentrations of $Ni(acac)_2$ as a function of irradiation time in the presence of sensitizer with or without Al_2O_3

that 84% of the nickel particles has a diameter ranging from 1 to 3 nm, with a monomodal distribution centered at 2 and 3 nm. TEM image (Fig. 2c) and relative size distribution (Fig. 2d) of Ni/Al_2O_3 (I) catalyst show analogous results with that of Ni/Al_2O_3 (P), although the average particle size was between 1 and 2 nm.

Figure 3 shows the variation of ζ potential with pH for Ni/Al_2O_3 (P) and Ni/Al_2O_3 (I) slurries, in the absence of 2,4-D model compound (fresh). It is well-known that the Al_2O_3 is an amphoteric catalyst with Lewis acid AlOH(H+) sites and basic Al–OH sites which play an important role in the catalytic ozonation reaction. According to our results, the Ni/Al_2O_3 (P) has a basic character demonstrated by its pH_{pzc} of 9, while Ni/Al_2O_3 (I) has a lower value of 8. As reported in the experimental section, the catalytic ozonation was carried out at pH = 3.1, which means that the surface of both catalysts should be charged positively. This surface transformation can favor the formation of OH radicals, due to the interaction with ozone, as proposed by Vittenet et al. 2015.

The present X-ray photoelectron spectroscopy (XPS) analysis compares surface chemical characteristics of catalysts produced by the photodeposition (P) and impregnation (I) methods using $Ni(acac)_2$ as Ni precursor and alumina as a support. The alumina support (Al_2O_3) was analyzed before and after ozonation reaction (Al_2O_3–O_3). All XPS spectra were charge corrected to the binding energy of –C–C, –CH carbon species at 284.6 ± 0.1 eV. Survey spectra (not shown) revealed the expected chemical elements: Al, O, C, and Ni. Figure 4 shows high resolution Al 2p, O 1s, C 1s, and Ni 2p XPS spectra for Al_2O_3, Al_2O_3–O_3, and catalysts: Ni/Al_2O_3 (P) and Ni/Al_2O_3 (I). Figure 4a, b displays the Al 2p (74.0 eV, FWHM: 1.9 eV) and O 1s (530.9 eV, FWHM: 2.5 eV) peaks for support before ozonation, Al_2O_3. The shape of these peaks is about symmetrical. The corresponding peaks for support after ozonation, Al_2O_3–O_3, and catalysts before reaction, Ni/Al_2O_3 (P) and Ni/Al_2O_3 (I), are similar to Al_2O_3 in position, width, and shape. This result shows that the Al_2O_3 surface is stable upon the oxidizing reaction conditions and nickel deposition processes. Though, small concentration changes are detected. Table 1 displays the corresponding quantification.

The Al:O ratio in Al_2O_3 is 2:3.3, somewhat larger than stoichiometric (2:3), typical of a hydrated surface oxide. For Al_2O_3–O_3, the Al:O ratio (2:3.5) is slightly larger than for Al_2O_3. Hydrating effects from the reaction media could explain the oxygen concentration increase; however, no significant differences (binding energy, width, or shape) are observed on the O 1s peaks that can confirm extra oxygen species; perhaps the difference in oxygen species is subtle.

Alternatively, reaction byproducts, most likely oxidized carbon species, could account for the oxygen concentration increase. The corresponding C 1s spectra are presented in Fig. 4c. After deconvolution, peaks for

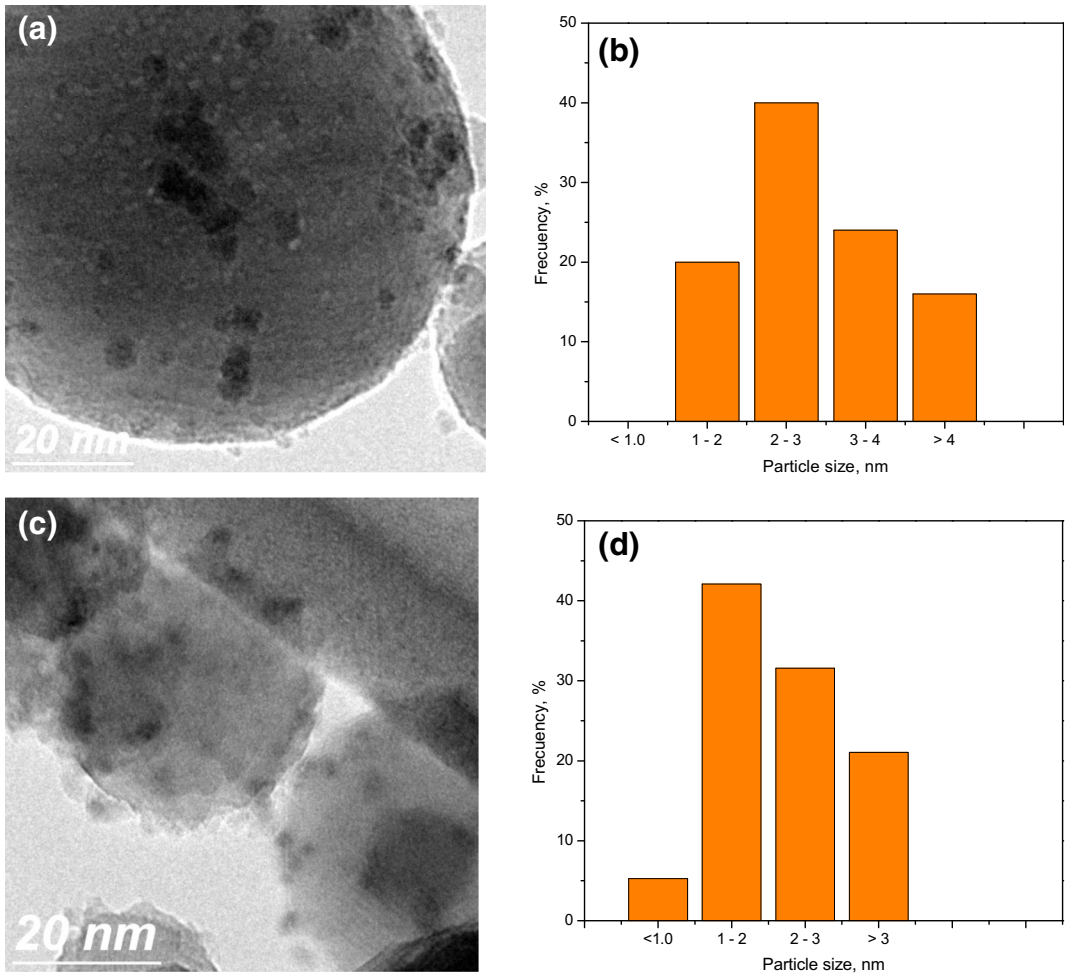

Fig. 2 TEM micrographs and nickel oxide particle size distribution of alumina-supported Ni catalysts. Ni/Al_2O_3 (P) (**a** and **b**) and Ni/Al_2O_3 (I) (**c** and **d**)

–C–C, –C–H (284.6 eV ± 0.1 eV), –COH (286.2 ± 0.2 eV), –C=O (287.3 ± 0.2 eV), and –HOC=O (288.9 ± 0.2 eV) are found. While the C concentration is almost the same as in Al_2O_3 (Table 1), the contribution of oxidized carbon species increased by 5.5% (compared to Al_2O_3). The Al:O ratio (2:3.2) for Ni/Al_2O_3 (P) is smaller than for Al_2O_3, as it was dried at 120 °C, while for Ni/Al_2O_3 (I) the ratio is the smaller one, as it was calcined at 500 °C. The C concentration for Ni/Al_2O_3 (P) is a little larger than for Ni/Al_2O_3 (I), but still noticeable. Nevertheless, more differences can be observed in the distribution of oxidized carbon species, specifically –COH and –C=O (Fig. 3c). In Ni/Al_2O_3 (P), the ratio –COH:–C=O is 0.4:1, conversely, for Ni/Al_2O_3 (I), it is 4:1. Clearly, the carbon contributions are of a different nature. These differences can be explained in terms of the nickel deposition methods: photodeposition and impregnation, as follows. Figure 4d shows the Ni 2p XPS signal for both catalysts. The fitting criterion was based on (Prieto et al. 2012; Biesinger et al. 2009; Moulder et al. 1995), where satellites are taken into account. The main contribution comes from $Ni(OH)_2$, followed by $Ni(acac)_2$, and minor peaks for NiO and Ni°. These species were also found in a previous work for nickel photodeposited on silica, NiO/SiO_2 (P), using the same synthesis method (Rodríguez et al. 2014). In the present case, the $Ni(acac)_2$ component is not as large, though this is an important difference because it points out that alumina improves the decomposition of $Ni(acac)_2$ (nickel precursor), in comparison with silica. It has been demonstrated that $Ni(acac)_2$ is stable at 120 °C when supported in alfa-alumina (Molina and Poncelet 1999), which is our drying temperature. Thus, it can be said that the photodeposition treatment

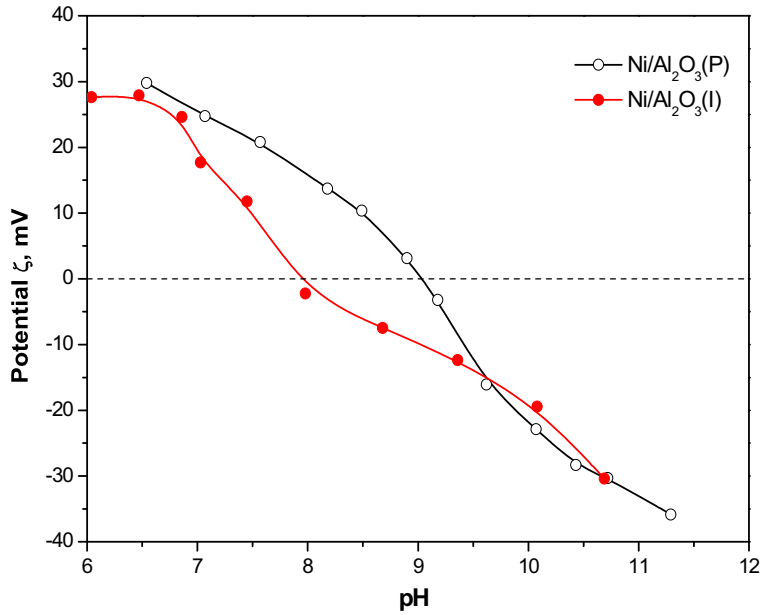

Fig. 3 The variation of ζ potential with pH for Ni/Al_2O_3 (P) and Ni/Al_2O_3 (I)

decomposes the nickel precursor, leading to the above mentioned nickel species. However, it is hard to stabilize small metallic Ni particles because they are reoxidized readily by ambient air, see below. On the other hand, the acetylacetonate anion contains –C=O groups (metal ligand), thus, partially or not decomposed nickel precursor left on the support surface will contribute to the –C=O XPS signal, as seen in the corresponding C 1s deconvolution. In the case of Ni/Al_2O_3 (I), the main contribution comes from $Ni(OH)_2$ and, similarly to Ni/Al_2O_3 (P), small peaks for NiO and Ni° are found. This result is also comparable to nickel impregnated on silica and reduced in hydrogen at 500 °C, NiO/SiO_2 (I), (Rodríguez et al. 2014). Again, this comportment has been reported (Karmhag et al. 2001; Uchikoshi et al. 1994), nickel nanoparticles form an oxide layer (~2.3 nm in thickness) in air at room temperature. The oxide is comprised of NiO (inner layer) and $Ni(OH)_2$ (outer layer). Being XPS surface sensitive, a spectrum dominated by $Ni(OH)_2$ is observed. In this case, since no carbon species are associated to nickel, the C 1s signal should be different, as seen in Fig. 4c. This confirms that our Ni 2p and C 1s deconvolutions are reasonable. Finally, the C/Ni ratio for NiO/SiO_2 (P) and NiO/SiO_2 (I) is 31.2 and 13.4, respectively. For the case of Ni/Al_2O_3 (P) and Ni/Al_2O_3 (I), that ratio is much lower, 12.7 and 7.0. That is about half as much carbon for both of the deposition methods. This comparison manifests that the support plays an active role during the nickel deposition, confirming the results presented in Fig.1.

Catalytic ozonation activity

As mentioned before, the catalytic ozonation to remove toxic organic compounds in aqueous solution employing Al_2O_3 has had a growing interest (Guzman-Perez et al. 2012; Pocostales et al. 2011; Rosal et al. 2010; Yang et al. 2010; Yang et al. 2009). For example, Qi et al. 2008 and Ernst et al. 2004 reported that the catalytic ozonation with alumina can be explained in terms of its adsorption capacity to transform ozone into free radicals, where the active sites are surface hydroxyl groups. To evaluate the catalytic effect on ozonation, the degradation efficiency of 2,4-D in presence of catalyst and ozone was investigated. A 95% of initial herbicide concentration was eliminated by ozone with Ni/Al_2O_3 (P and I) catalysts during 15 min (not shown). Figure 5a shows the 2,4-D decomposition initial reaction rates in the presence of the supported catalysts. Note that the Ni/Al_2O_3 (P) initial reaction rate was almost double than that of Ni/Al_2O_3 (I). In general, at increasing metal loading, the catalytic activity is improved until the optimal value. However, the photodeposited catalyst containing only 1 wt% Ni species showed a zero point charge value of 9, whereas, the impregnated catalyst was 8 pH_{pzc} almost similar than that of alumina (not shown here). This means that Ni species produced by

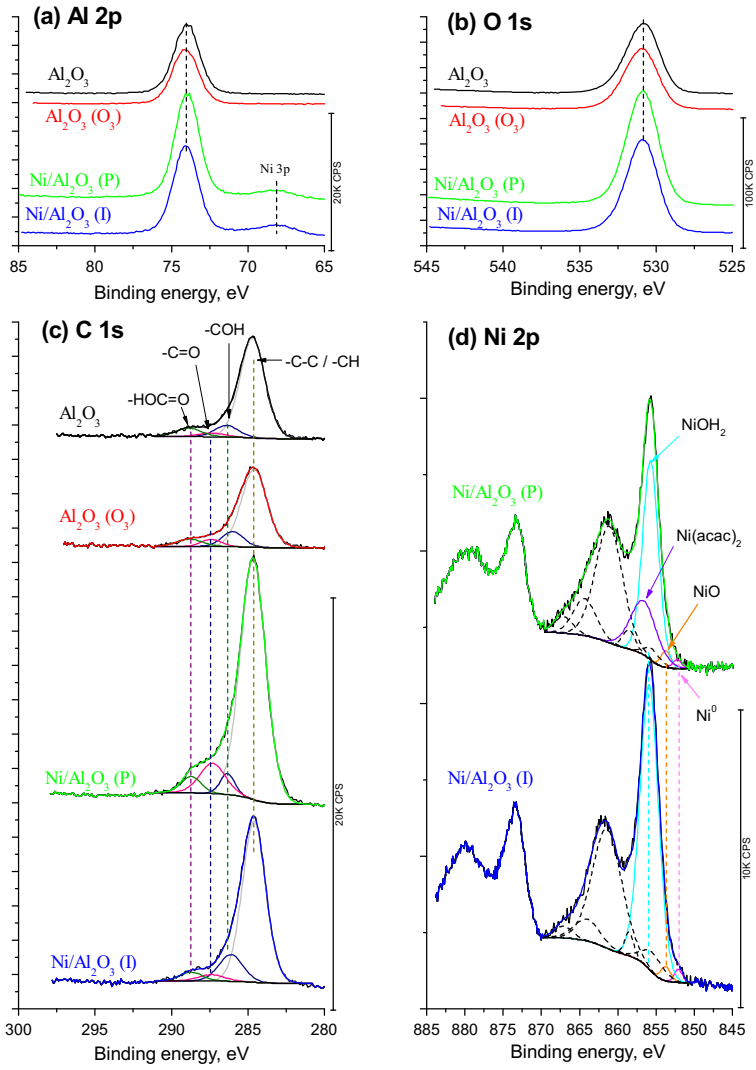

Fig. 4 High resolution **a** Al 2p, **b** O 1s, **c** C 1s, and **d** Ni 2p XPS spectra for support before, Al_2O_3, and after, Al_2O_3-O_3, ozonation reaction and for as-prepared catalysts: Ni/Al_2O_3 (P) and Ni/Al_2O_3 (I)

the photodeposited catalyst increase the surface hydroxyl groups leading to a higher production of oxidant agents (Vittenet et al. 2015). In addition, one identified byproduct (maleic acid) during the herbicide removal in the presence of both catalysts is reported in Fig. 5b. It is worth noting that the higher amount of maleic acid was produced by the Ni/Al_2O_3 (P) catalyst which confirms a higher population of oxidant agents in this solid.

Table 1 Atomic concentration for chemical elements in support (before and after ozonation reaction) and contribution from carbon species found in the C 1s XPs signal

Sample	Atomic concentration					Contribution from carbon species				
	% Al	% O	Al:O	% C	% Ni	% [–C–C,–C–H]	% [–COH]	% [–C=O]	[–COH]:[–C=O]	% [–HOC=O]
Al_2O_3	33.3	54.5	2:3.3	12.2	–	80.6	8.9	3.3	2.7:1	7.2
Al_2O_3– O_3	31.8	55.8	2:3.5	12.4	–	75.1	12.2	5.4	2.3:1	7.3
Ni/Al_2O_3 (P)	30.8	50.0	2:3.2	17.8	1.4	81.4	4.0	10.3	0.4:1	4.3
Ni/Al_2O_3 (I)	32.7	50.4	2:3.1	14.8	2.1	79.0	13.5	3.4	4: 1	4.1

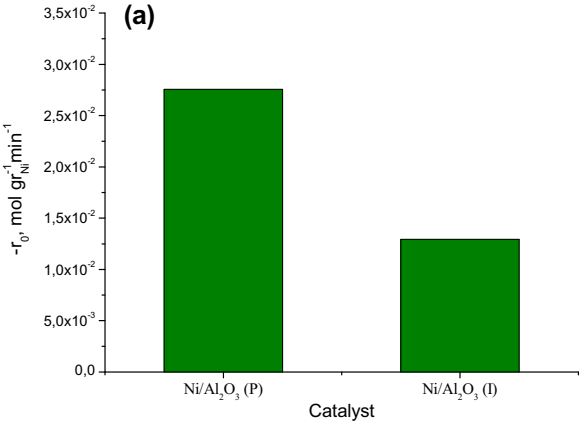

Fig. 5 **a** Initial reaction rates obtained in the catalytic ozonation of 2,4-D in aqueous solution and **b** concentration profiles of maleic acid (byproduct generated during 2,4-D degradation). *Experimental conditions:* $[O_3] = 25 \pm 3$ mg L^{-1}, [Catalyst] = 0.1 gL^{-1}, [2,4-D] = 80 mgL^{-1}, pH = 3.1

Kinetic study

Reaction constants of 2,4-D decomposition by ozone were determined in acid condition, considering the overall reaction order as second degree. That is, the kinetic study considered the dependence of reaction condition on both, the ozone (gas phase at the reactor outlet) and the herbicide concentrations (see eq. 1).

$$-C_{2,4-D} = kC_{2,4-D}C_{O_3} \quad (1)$$

$$C_{2,4-D} = -k_1 C_{2,4-D}C_{O_3} - k_2 C_{2,4-D}C_{\cdot OH} \quad (2)$$

$$C_{O_3} = -k_1 C_{2,4-D}C_{O_3} - k_3 C_{cat}C_{O_3} - \sum_{i=1}^{n} k_{pi}C_i C_{O_3} \quad (3)$$

$$C_{\cdot OH} = k_3 C_{cat}C_{O_3} - k_2 C_{2,4-D}C_{\cdot OH} - C_{\cdot OH}\sum_{i=1}^{n} k_{qi}P_i - k_5 C_{\cdot OH} \quad (4)$$

$$\sum_{i=1}^{n} \dot{P}_i = C_{O_3}\sum_{i=1}^{n} k_{fi}C_{2,4-D} - C_{O_3}\sum_{i=1}^{n} k_{pi}P_i - \sum_{i=1}^{n} k_{qi}C_{OH}P_i \quad (5)$$

The bimolecular constants were determined with information of dissolved ozone concentration in gas phase as well as 2,4-D and byproducts concentration profiles (not shown here) with the model developed in (Poznyak et al. 2005). To explain the reaction conditions when the catalyst participates in the reaction, the model considered the herbicide dynamics ($C_{2,4\text{-}D}$), the dissolved ozone (C_{O3}), free radicals ($C_{\cdot OH}$) and byproducts obtained during the reaction (C_{Pi}). The herbicide decomposition considered two effects: the herbicide degradation by the direct mechanism (modeled as a bimolecular reaction) and the OH radical effect (indirect mechanism) modeled in Eq. 2. The constant k_1 represents the reaction rate constant between ozone and the herbicide while k_2 represents the reaction rate constant between the 2,4-D and OH radicals. Three effects were considered by studying the variation of ozone concentration in the liquid phase: (a) depletion of ozone concentration by its reaction with 2,4-D, (b) ozone decomposition by the presence of the catalyst, and (c) ozone consumption by the decomposition of byproducts. Self-decomposition of ozone is relatively slow with respect to the previous phenomena; therefore, it was not considered (see Eq. 3) where k_3 is the reaction rate constant between catalyst concentration and ozone, while k_{Pi} represents the reaction rate constants based on the degradation byproducts.

Table 2 Reaction rate constant obtained with the model in presence of catalysts supported Al_2O_3

Compound	k, L gr_{Ni}^{-1} mol^{-1} s^{-1}	
	Ni/Al_2O_3 (P)	Ni/Al_2O_3 (I)
2,4-D	9.380×10^6	4.400×10^6
2,4-DCP	0.404×10^6	0.392×10^6
Maleic acid	6.850×10^3	6.033×10^3
Oxalic acid	-2.300×10^6	-0.072×10^6

Equation 4 shows the variation of OH radicals concentration generated by the effect of the catalyst on the ozone decomposition carried out the herbicide elimination and the byproducts generated. Also, there is also recombination effect of the OH radicals where k_5 is rate reaction constant relative to the OH radical recombination while k_{qi} express byproducts decomposition by OH radicals. Equation 5 represents the reaction rate of the byproducts decomposition arising of the catalytic ozonation. The first term represents the formation of byproducts by the 2,4-D decomposition, the second factor is due to the decomposition of them by conventional ozonation, and the latter represent the byproducts interaction with OH radicals. All these constants are expressed in L gr_{Ni}^{-1} mol^{-1} s^{-1}, and they are reported in Table 2. These constants were obtained using the parametric identification method reported in (Poznyak et al. 2005).

The kinetic constants reported in the previous table represent the compound decomposition, except oxalic acid which is formation constant, because this byproduct was not eliminated at all under the reaction conditions proposed in this study. In general, the kinetic constants calculated for the removal of the herbicide depend on the type of catalyst used in the reaction. In the case of byproducts, an increment of reaction rate constant was observed when the considered catalyst was Ni/Al_2O_3 (P).

Conclusions

Ni catalysts supported on alumina were prepared by photodeposition and impregnation methods. It was demonstrated that it is possible to carry out the photodeposition of Ni species (2–3 nm) on alumina by using UVA light (365 nm) and benzophenone as a sensitizer without any subsequent thermal treatment. The photodeposited catalysts (1 wt% Ni) showed almost double of initial activity than that of impregnated catalysts (3 wt%), though the particle size distribution was very similar for both catalysts, as well as their surface composition. For instance, the photodeposited catalyst presented $Ni(OH)_2$, $Ni(acac)_2$, NiO, and Ni°, the impregnated catalysts had a similar composition, excepting $Ni(acac)_2$. However, the photodeposited catalysts increased the zero point charge of alumina, from 8 to 9, while the impregnated did not modify its surface basicity. In summary, the higher catalytic activity and byproduct concentration (maleic acid) of the photodeposited catalyst can be explained in terms of a higher OH radical formation, improving the overall oxidation process.

Acknowledgements H. Tiznado would like to thank Eng. David Dominguez for the XPS support and UNAM PAPIIT 1N105114 and 1N107715 for the economic support. J.L. Rodriguez would like to thank the IPN (Project: SIP 20160762) for the economic support. M.A. Valenzuela would also like to thank the IPN (SIP-20161484) and Conacyt (153356).

Compliance with ethical standards

Conflict of interest The authors declare that they have no conflict of interest.

References

Avramescu SM, Bradu C, Udrea I, Mihalache N, Ruta F (2008) Degradation of oxalic acid from aqueous solutions by ozonation in presence of Ni/Al_2O_3 catalysts. Cat Commun 9: 2386–2391

Biesinger MC, Payne BP, Lau LWM, Gerson A, Smart RSC (2009) X-ray photoelectron spectroscopic chemical state quantification of mixed nickel metal, oxide and hydroxide systems. Surf Interface Anal 41:324–332

Crisafulli C, Scirè S, Giuffrida S, Ventimiglia G, Lo Nigro R (2006) An investigation on the use of liquid phase photodeposition for the preparation of supported Pt catalysts. Appl Catal A 306:51–57

Ernst M, Lurot F, Schrotter J-C (2004) Catalytic ozonation of refractory organic model compounds in aqueous solution by aluminum oxide. Appl Catal B 47:15–25

Gautam RK, Chattopadhyaya MC (2016) Advanced nanomaterials for wastewater remediation. CRC Press 1st Ed. 33–48

Giuffrida S, Condorelli GG, Costanzo LL, Ventimiglia G, Lo Nigro R, Favazza M, Votrico E, Bongiorno C, Fragala IL (2007) Nickel nanostructured materials from liquid phase photodeposition. J Nanopart Res 9:611–619

Guzman-Perez CA, Soltan J, Robertson J (2012) Catalytic ozonation of 2,4-dichlorophenoxyacetic acid using alumina in the presence of a radical scavenger. J Environ Sci Health B 47: 544–552

Ichikawa S-I, Mahardiani L, Kamiya Y (2014) Catalytic oxidation of ammonium ion in water with ozone over metal oxide catalysts. Cat Today 232:192–197

Ikhlaq A, Brown DR, Kasprzyk-Hordern B (2012) Mechanisms of catalytic ozonation on alumina and zeolites in water: formation of hydroxyl radicals. Appl Catal B 123–124:94–106

Ikhlaq A, Brown DR, Kasprzyk-Hordern B (2013) Mechanisms of catalytic ozonation: an investigation into superoxide ion radical and hydrogen peroxide formation during catalytic

ozonation on alumina and zeolites in water. Appl Catal B 129:437–449

Karmhag R, Niklasson GA, Nygren M (2001) Oxidation kinetics of nickel nanoparticles. J Appl Phys 89:3012–3017

Kometani N, Doi H, Asami K, Yonezawa Y (2002) Laser flash photolysis study of the photochemical formation of colloidal Ag nanoparticles in the presence of benzophenone. Phys Chem Chem Phys 4:5142–5147

Krylova GV, Eremenko AM, Smirnova NP, Eustis S (2005) Photogeneration of nanosized gold on the surface of mesoporous silica modified by benzophenone. Theor Exp Chem 41:365–370

Molina R, Poncelet G (1999) α-Alumina-supported nickel catalysts prepared with nickel acetylacetonate. 2. A study of the thermolysis of the metal precursor. J Phys Chem B 103: 11290–11296

Moulder JF, Stickle WF, Sobol PE, Bomben KD (1995) Handbook of x-ray photoelectron spectroscopy: a reference book of standard spectra for identification and interpretation of XPS data. Physical Electronics

Nawrocki J (2013) Catalytic ozonation in water: controversies and questions. Appl Catal B 142:465–471

Nawrocki J, Kasprizk-Hordern B (2010) The efficiency and mechanisms of catalytic ozonation. Appl Catal B 99:27–42

Nie Y, Hu C, Yang L, Hu J (2013) Inhibition mechanism of BrO_3^- formation over MnO_x/Al_2O_3 during the catalytic ozonation of 2, 4-dichlorophenoxyacetic acid in water. Sep Purif Tech 117:41–45

Pocostales P, Álvarez P, Beltrán FJ (2011) Catalytic ozonation promoted by alumina-based catalysts for the removal of some pharmaceutical compounds from water. Chem Eng J 168: 1289–1295

Poznyak T, Chairez I, Poznyak A (2005) Application of a neural observer to phenols ozonation in water: simulation and kinetic parameters identification. Water Res 39:2611–2620

Prieto P, Nistor V, Nouneh K, Oyama M, Abd-Lefdil M, Díaz R (2012) XPS study of silver, nickel and bimetallic silver–nickel nanoparticles prepared by seed-mediated growth. Appl Surf Sci 258:8807–8813

Qi F, Chen Z, Xu B, Shen B, Shen J, Ma J, Joll C, Heitz A (2008) Influence of surface texture and acid–base properties on ozone decomposition catalyzed by aluminum (hydroxyl) oxides. Appl Catal B 84:684–690

Qi F, Xu B, Chen Z, Feng L, Zhang L, Sun D (2013) Catalytic ozonation of 2-isopropyl-3-methoxypyrazine in water by γ-AlOOH and γ-Al_2O_3: comparison of removal efficiency and mechanism. Chem Eng J 219:527–536

Rodríguez JL, Valenzuela MA, Tiznado H, Pola F, Tiznado H, Poznyak T (2012) Photodeposition of Ni nanoparticles on TiO_2 and their application in the catalytic ozonation of 2,4-dichlorophenoxyacetic acid. J Mol Catal A 353:29–36

Rodríguez JL, Valenzuela M, Poznyak T, Lartundo L, Chairez I (2013) Reactivity of NiO for 2,4-D degradation with ozone: XPS studies. J Hazard Mat 262:472–481

Rodríguez JL, Valenzuela M, Tiznado H, Poznyak T, Flores E (2014) Synthesis of nickel oxide nanoparticles supported on SiO_2 by sensitized liquid phase photodeposition for applications in catalytic ozonation. J Mol Catal A 392:39–49

Rosal R, Gonzalo MS, Rodríguez A, García-Calvo E (2010) Catalytic ozonation of fenofibric acid over alumina-supported manganese oxide. J Hazard Mater 183:271–278

Sakamoto M, Fujistuka M, Majima T (2009) Light as a construction tool of metal nanoparticles: synthesis and mechanism. J Photochem Photobiol C 10:33–56

Scirè S, Crisafulli C, Giuffrida S, Mazza C, Riccobene PM, Pistone A, Ventimiglio G, Bongiorno C, Spinella C (2009) Supported silver catalysts prepared by deposition in aqueous solution of Ag nanoparticles obtained through a photochemical approach. Appl Cat A 367:138–145

Scirè S, Giuffrida S, Crisafulli C, Riccobene PM, Pistone A (2011) Direct and sensitized liquid phase photodeposition for the preparation of alumina supported Pd nanoparticles for applications to heterogeneous catalysis. J Nanopart Res 13:3217–3228

Scirè S, Giuffrida S, Crisafulli C, Riccobene PM, Pistone A (2012) Liquid phase photo-deposition in the presence of unmodified β-cyclodextrin: a new approach for the preparation of supported Pd catalysts. J Mol Catal A 353–354:87–94

Uchikoshi T, Sakka Y, Yoshitake M, Yoshihara K (1994) A study of the passivating oxide layer on fine nickel particles. Nanostructured Mater 4:199–206

Vittenet J, Aboussaoud W, Mendret J, Pic JS, Debeffefontaine H, Lessage N, Faucher K, Manero M-H, Starzyk FT, Leclerc H, Galarneau A, Brosillon S (2015) Catalytic ozonation with γ-Al_2O_3 to enhance the degradation of refractory organics in water. Appl Catal A 504:519–532

Yang L, Hu C, Nie Y, Qu J (2009) Catalytic ozonation of selected pharmaceuticals over mesoporous alumina-supported manganese oxide. Environ Sci Technol 43:2525–2529

Yang L, Hu C, Nie Y, Qu J (2010) Surface acidity and reactivity of β-FeOOH/Al_2O_3 for pharmaceuticals degradation with ozone: in situ ATR-FTIR studies. Appl Catal B 97:340–346

Zhang T, Li W, Crové J-P (2012) A non-acid-assisted and non-hydroxyl-radical-related catalytic ozonation with ceria supported copper oxide in efficient oxalate degradation in water. Appl Catal B 121:88–94